

# Microlensing Parallax for Observers in Heliocentric Motion

S. Calchi Novati<sup>1,2,3,a</sup>, G. Scarpetta<sup>2,3</sup>

## ABSTRACT

Motivated by the ongoing *Spitzer* observational campaign, and the forthcoming K2 one, we revisit, working in an heliocentric reference frame, the geometrical foundation for the analysis of the microlensing parallax, as measured with the simultaneous observation of the same microlensing event from two observers with relative distance of order AU. For the case of observers at rest we discuss the well known fourfold microlensing parallax degeneracy and determine an equation for the degenerate directions of the lens trajectory. For the case of observers in motion, we write down an extension of the Gould (1994) relationship between the microlensing parallax and the observable quantities and, at the same time, we highlight the functional dependence of these same quantities from the timescale of the underlying microlensing event. Furthermore, through a series of examples, we show the importance of taking into account the motion of the observers to correctly recover the parameters of the underlying microlensing event. In particular we discuss the cases of the amplitude of the microlensing parallax and that of the difference of the timescales between the observed microlensing events, key to understand the breaking of the microlensing parallax degeneracy. Finally, we consider the case of the simultaneous observation of the same microlensing event from ground and two satellites, a case relevant for the expected joint K2 and *Spitzer* observational programs in 2016.

*Subject headings:* gravitational lensing: micro

---

<sup>1</sup>NASA Exoplanet Science Institute, MS 100-22, California Institute of Technology, Pasadena, CA 91125, USA

<sup>2</sup>Dipartimento di Fisica “E. R. Caianiello”, Università di Salerno, Via Giovanni Paolo II, 84084 Fisciano (SA), Italy

<sup>3</sup>Istituto Internazionale per gli Alti Studi Scientifici (IIASS), Via G. Pellegrino 19, 84019 Vietri Sul Mare (SA), Italy

<sup>a</sup>Sagan Visiting Fellow

## 1. Introduction

The microlensing parallax is a key observable to break the degeneracy in the microlensing parameter space and recover the physical parameters of the lens, specifically its mass and distance. The framework for the analysis of the microlensing parallax, through measures from two observers distant enough one from the other, specifically through the simultaneous observation of the same microlensing event from ground and from space, has been set by Refsdal (1966) and later put up to date and developed by Gould (1994). The era of space-based microlensing-parallax observations started using *Spitzer* (Werner et al. 2004), as earlier suggested by Gould (1999), with the analysis of a SMC event (Dong et al. 2007), and later on continued with the ongoing *Spitzer* observational campaign started in 2014 for the follow up of microlensing events detected towards the Galactic bulge led by A. Gould (Gould et al. 2013, 2014, 2015a,b). This observational campaign has already led to several important results assessing clearly the importance of this kind of measurements, among which the first microlensing exoplanetary system with a space-based parallax measurement (Udalski et al. 2015); the first space-based microlens parallax measurement of an isolated star (Yee et al. 2015b); and a first analysis on one of the main goals of the campaign, the determination of the Galactic distribution of exoplanets (Calchi Novati et al. 2015a) (for this specific issue we also refer to the recent analysis by Penny et al. 2016). Furthermore, the space-based microlensing parallax is expected in the next few years to play an increasingly relevant role for the analysis of microlensing events, in particular for the characterization of exoplanets, besides *Spitzer* also with K2 (Howell et al. 2014) and, in the longer term, with WFIRST (Spergel et al. (2015), for specific analyses on the microlensing parallax with WFIRST we refer to Gould 2013; Yee 2013).

A key aspect in the analysis of space-based microlensing parallax events is the understanding of the underlying degeneracy for the parallax determination: a fourfold degeneracy of the direction of the parallax “vector” and a twofold degeneracy of the parallax amplitude which is the relevant quantity for the determination of the physical characteristics of the lens system. As further detailed below, this degeneracy arises because the observation of the same microlensing event from two observers only partly breaks the degeneracy among the directions of the lens-source relative motion, a degeneracy which is instead complete for the observation by a single observer of a single lens microlensing event. Gould (1994) set the framework, which has been followed thereafter, for the analysis of the microlensing parallax in the case of two inertial observers at rest. Gould (1995) then addressed also the issue of the parallax degeneracy for the case of two observers in relative motion, but still from within the framework established for the case of inertial observers at rest. The results of these works then became the basis for the analysis of the mechanism for breaking the parallax degeneracy, and in particular for two simulations of the microlensing parallax signal towards

the Magellanic Clouds (Boutreux & Gould 1996) and the Galactic bulge (Gaudi & Gould 1997). Incidentally, we recall that these are two opposite observational targets as they lie, roughly, at the ecliptic pole and along the ecliptic plane, respectively, the second line of sight being therefore coplanar with typical satellite orbits, and specifically for that of *Spitzer* and *Kepler*.

The recently renewed and growing observational importance of space-based microlens parallax calls for a better theoretical understanding of its underlying mechanisms in particular for the breaking of the degeneracy for observers in relative motion. Addressing this issue is the primary goal of the present work. Specifically, as a main result, we extend the Gould (1994) expression relating the microlens parallax to the light curve observable valid for observers at rest to the general case of observers in motion. Considering primarily the line of sight towards the Galactic bulge, currently the more relevant from an observational point of view, we then present a series of microlensing event test cases to show the impact of fully including in the analysis the motion of the observers comparing in particular with the outcome of the Gould (1995) analysis. As detailed below, we perform our analysis from within an heliocentric frame, therefore from the ideal point of view of an observer which can be to excellent approximation considered inertial. This choice, opposite to the usual one of a geocentric point view, allows us a more clear and transparent discussion of the problem.

The microlens parallax is a genuine geometrical effect. The strength of its measure with simultaneous ground and space-based observations is then enhanced by its clean signature on the light curves, resulting usually in rather precise determinations (the typical relative error for the parallax in single-lens systems in Calchi Novati et al. (2015a) is about 10%). Besides the error on the single parallax solutions, however, a major source of uncertainty remains that associated with the discrete degeneracy in the microlensing parallax determination. In this framework, to the extent that they may lead to break this degeneracy, this is where combined space-based analyses, as the expected joint observations with *Spitzer* and K2, may be expected to be of key importance. Considering the determination of the physical lens parameters, in particular the lens mass, we recall however that the measure of the microlensing parallax alone, besides the event duration, is not sufficient to break the degeneracy in the microlensing parameter space. The overall error budget for the physical parameters is therefore the result of the combined effect of all the measurable quantities. The degeneracy may be broken if, beside the microlensing parallax, the finite source effect, and therefore the Einstein angular radius, is also known. This is routinely measured in multiple-lens, planetary, systems, but only infrequently in single-lens ones. Out of the 2015 *Spitzer* campaign (Calchi Novati et al. 2015b), Zhu et al. (2015) report two such (single-lens system) cases, achieving a relative error for the lens mass of 15% and 8%. The two planetary systems with *Spitzer*-based microlens parallax, OGLE-2014-BLG-0124 (Udalski et al. 2015)

and OGLE-2015-BLG-0966 (Street et al. 2015), come with a relative error in the planet mass determination of 30% and 10%, respectively where, in the first case, the error budget is dominated by the uncertainty related to the finite source effect. We also recall that an alternative, and for ground-based observations only more generally applicable, channel to the determination of the physical parameters of lens systems, independent from the measure of the microlens parallax, is that associated to the measure, within a few years of the microlensing event itself, of both the lens flux and the relative lens-source proper motion (the second being key to unambiguously disentangle the lens and the source flux, Henderson et al. 2014). This kind of analysis requires high angular resolution imaging facilities, ground-based adaptive optic systems or space observatories, eg the *HST*: in this framework Bennett et al. (2015) and Batista et al. (2015) have recently reported on their analyses of the planetary system OGLE-2005-BLG-169 (Gould et al. 2006) where they reach a precision of 6% in the planet mass determination.

The paper is organized as follows. In Section 2 we set the framework of our analysis; in Section 2.1 we describe the case of the microlensing parallax for two observers at rest within an heliocentric frame, and in particular we go through a detailed geometrical analysis of the underlying degeneracies; in Section 2.2 we extend the analysis to the case of observers in motion; in Section 3 we present an analysis of the parallax for a sample of light curves, for the line of sight towards the Galactic Bulge; finally, in Section 4 we discuss the case for the simultaneous observation of the same microlensing event from ground and two satellites, which is the exciting case we expect to happen during the K2 and *Spitzer* microlensing campaign in 2016.

## 2. The microlensing parallax

We start by setting the framework and the notation of our analysis. Through the paper we consider a single-point source single-lens system. A microlensing event (for a review see for instance Mao 2012) is then characterized by three parameters: the time at maximum magnification,  $t_0$ , the impact parameter,  $u_0$ , which sets the magnification at maximum along the microlensing light curve at  $t = t_0$ , and the *Einstein time*,  $t_E$ , which sets the timescale of the event. The light curve magnification, the typical bell-like symmetric shape known as Paczyński light curve (Paczynski 1986), reads

$$A(t) = A(u(t)) = \frac{u^2 + 2}{u\sqrt{u^2 + 4}}, \quad u(t) = \sqrt{u_0^2 + \left(\frac{t - t_0}{t_E}\right)^2}, \quad (1)$$

where  $u(t)$  describes the relative distance, projected on the lens plane orthogonal to the line of sight to the source, of the lens with respect to the observer.

The expression for  $u(t)$  in Eq. 1 holds for linear uniform lens motion with respect to an inertial observer; it is an excellent approximation for typical microlensing events, lasting from days up to few months, for an ideal observer on the Sun. Furthermore, Eq. 1 works well also for observers on Earth, except for very long timescale events, where the orbital motion comes into play.

All the physical parameters of the source-lens system are enclosed in the event timescale, the *Einstein time*  $t_E = R_E/v$ , where  $v$  is the relative lens-source velocity on the lens plane. The *Einstein radius*,  $R_E$ , is the characteristic length of the system, with all the physical lengths on the lens plane being normalized with it. The Einstein radius is a function of the distance from the observer to the lens,  $D_l$ , the source,  $D_s$ , and of the lens mass,  $M_l$ . The *microlensing parallax*,  $\pi_E$ , is defined as the inverse of the Einstein radius, in units of AU, projected on the observer plane,  $\pi_E = \text{AU}(1 - x)/R_E$ , where  $x \equiv D_l/D_s$ . We recall that for Galactic bulge events typically  $R_E$  is of order AU. (This is the underlying reason why, to measure the microlensing parallax, the two observers must lie at about a relative distance of order AU. The exception are the rare cases of extremely highly magnified microlensing events for which the microlensing parallax can be determined from two observers separated by about 1 Earth radius, Gould 1997). We recall that the choice of the microlensing parameters is not univocal, in particular the formalism can be more suitably (for several applications) recasted in terms of observables (Gould 2000).

In principle one may further characterize a microlensing event by giving, additionally, the direction of the lens relative motion in the lens plane, which however remains completely undetermined in Eq. 1, which only contains the modulus of the impact parameter. The direction of motion is however relevant when discussing the parallax, so that we here introduce, as a fourth parameter, the angle  $\chi$  between a fixed direction (in our notation, the  $x$ -axis of the reference frame to be introduced in Section 2.1) and the orthogonal to the direction of the lens motion.

The three parameters  $t_0$ ,  $u_0$  and  $\chi$  all characterize the geometry of the microlensing event. The first two do not carry any information on the physical parameters of the lens system, their underlying distribution is indeed flat. The case of  $\chi$  is different, though, as its distribution reflects that of the underlying lens and source velocity and therefore is endowed with an intrinsic, often relevant, physical information<sup>1</sup>.

Note finally that in the following we will always refer to the microlensing parameters  $t_0$ ,  $u_0$  and  $t_E$ , without further subscript, as those of the underlying microlensing event as

---

<sup>1</sup>From an observational point of view also the distribution for  $u_0$  is not flat. This reflects both the efficiency of a given instrumental setup and therefore, indirectly, also the underlying source luminosity function.

would be seen from the ideal observer on the Sun.

## 2.1. Observers at rest in an heliocentric reference system

In this section we revisit the analysis of the microlensing parallax with observers at rest within an heliocentric framework. This approach provides us with a different point of view on well known results and, at the same time, leads us to highlight some relationships which, to our knowledge, may not have been already discussed. Furthermore, this gives us the necessary basis for the discussion of the case with observers in motion.

We are going to consider an heliocentric cartesian frame on the lens plane, centered along the line of sight to the source, as seen from the Sun. The choice of the reference frame within the lens plane is then arbitrary modulus a rotation in this plane. The orbital motions of the observers we are going to discuss all take place on the ecliptic plane which therefore takes a privileged position. The “canonical” choice for the reference frame in the lens plane, from a geometrical point of view, would then be that of having one of the axes pointing along the line of nodes, intersection of the ecliptic plane with the lens plane. Following the established habit in literature, however, we fix the  $x$ -axis along the line of nodes intersection of the lens plane with the equatorial plane instead, with in particular the  $x$  and  $y$  axes pointing along the equatorial coordinates, west and north, respectively. We note however that because the line of sight we consider is pointing towards the Bulge, roughly on the ecliptic plane and at  $\lambda \sim 270^\circ$ , these two choices almost coincide.

Let us consider an observer at rest out of the origin, which can be the Earth approximated at rest. Its position in the lens plane, as given by the intersection of its line of sight to the source with the lens plane, then depends, besides from its position in the observer plane, only on the microlensing parallax. Specifically, its distance from the origin scales with the microlensing parallax<sup>2</sup>. Because of his offset from the origin, this observer would observe the same microlensing event as seen from the (ideal) observer in the origin, with the same timescale  $t_E$ , but with different impact parameter and time at maximum magnification. Let introduce a second observer lying into the same observer plane, which for definiteness we are going to identify with the satellite *Spitzer*, and which for now we also consider to be at rest. The relative distance between the two observers, a known quantity in the observer plane,

---

<sup>2</sup>From an analytical point of view, this holds within the usual approximation of neglecting the lengths in the observer plane, of order AU, compared to the distance to the source, of order kpc. We note that this is the same approximation within which we can mix up geocentric and heliocentric equatorial coordinates.

when projected in the lens plane also scales with the microlensing parallax (Gould 1994)

$$\begin{aligned}\vec{\pi}_E &= \vec{\pi}_{E,\pm,\pm} = \frac{\text{AU}}{D_\perp} (\tau, \Delta u_{0,\pm,\pm}) , \\ \tau &= \frac{t_{0,2} - t_{0,1}}{t_E} , \quad \Delta u_{0,\pm,\pm} = \pm(|u_{0,2}| \pm |u_{0,1}|) .\end{aligned}\tag{2}$$

Here  $t_{0,1}$ ,  $t_{0,2}$  and  $u_{0,1}$ ,  $u_{0,2}$  indicate the time at maximum magnification and the impact parameter of the microlensing event as seen by the two observers, and  $D_\perp$  is the relative physical distance between the two observers in the lens plane, expressed in AU. For reference, in the following we will always identify the observer “1” as that on Earth. This expression is key for the measurement of the microlensing parallax which is there expressed in terms of all observable quantities.

The basis of Eq. 2 lies on elementary geometrical considerations which can be done for instance looking at Figure 1, further discussed below. The notations  $\pm, \pm$  in Eq. 2 refers to the aforementioned fourfold degeneracy in the vector parallax determination, and twofold degeneracy in the modulus,  $\pi_{E,\pm}$ , which we now describe in some detail.

In Figure 1 we represent the (four degenerate configurations for the) geometry of a microlensing event projected on the lens plane as seen by the two observers (Earth and *Spitzer*). Centered on the origin we draw a circle of radius  $u_0$ . From the point of view of the ideal observer in the origin (the Sun) the observed light curve is compatible with whatever lens motion direction tangent to this circle. The angle  $\chi$ , though, singles out a unique lens direction, with the lens passing at the tangent point at time  $t_0$ . We can draw similar circles around the observer positions on the lens plane, with radius  $u_{0,1}$  and  $u_{0,2}$  respectively. Geometrically, the lens trajectory must then be tangent simultaneously to all the three circles, with  $t_{0,1}$  and  $t_{0,2}$  being the times of passage of the lens at the respective tangent points.

Following the habit (and with some abuse of notation) in Eq. 2 we have introduced the parallax “vector”,  $\vec{\pi}_E$ , with components projected along and perpendicular to the lens motion. The amplitude of the parallax vector, the microlensing parallax  $\pi_E$ , is then obtained applying the Pythagoras theorem to the right angle triangle whose hypotenuse is given by the distance between the two observers, and whose cathetus are equal respectively to the distance between the tangent points of the two observer circles and to the difference of the observers impact parameters (Figure 1, top panels).

Let us pause to write down an expression for  $\tau = \Delta t_0/t_E$  as a function of the parameters of the underlying microlensing event

$$\tau = \pi_E (\cos(\chi)\Delta y_0 - \sin(\chi)\Delta x_0) ,\tag{3}$$

where  $(\Delta x_0, \Delta y_0)$  are the distances of the observers position projected on the lens plane, with  $D_\perp$  in Eq. 2 equal to  $\sqrt{(\Delta x_0)^2 + (\Delta y_0)^2}$ . In Eq. 3  $\Delta t_0$ ,  $\Delta x_0$  and  $\Delta y_0$  are all to be intended as signed quantities, as well as  $t_E$ , whose sign can be thought to identify the versus of motion along a given direction. Specifically, our sign convention is that, looking the lens plane as in Figure 1, the lens motion is anti-clockwise at the tangent point between the lens trajectory and the circle of radius  $u_0$  centered in the origin. We also note that  $\tau$  is invariant upon change of the direction of motion (which corresponds to a simultaneous change of the sign of  $t_E$  and therefore also of  $\Delta t_0$ ). Eq. 3 follows from the geometry of the problem and is therefore implicit in Eq. 2 (in particular it is closely related to Eq. 8 in Gould 2004) however to our knowledge it was not previously explicitly written down. In particular it relates the projections of the components of  $D_\perp$  along the lens trajectory to the distance between the two tangent points to the observer circles, which is equal to the difference of the observers time at maximum magnification in units of the Einstein time (we recall that all the distances are normalized by  $R_E$ ). This equation is important as, together with Eq. 2, it provides the basic analytical understanding of the underlying fourfold degeneracy. Specifically, it makes transparent that  $\tau$  only depends, besides the known observers position, from  $\pi_E$  and  $\chi$ . Namely, besides being independent from the event timescale, which is obvious as the parallax is intrinsically a static quantity,  $\tau$  is also independent from the impact parameter and the time at maximum magnification of the underlying microlensing event. This is key to explain the parallax degeneracy. Fixed  $\tau$  and  $\pi_E$ , Eq. 3 can be looked at as an equation for  $\chi$ , and, in agreement with the geometry shown in Figure 1, it is a quadratic equation (see also Gould (2014) for a discussion of the widespread appearance of quadratic equations in microlens parallax). Namely, there are two possible lens trajectories compatible with the light curves as seen from the two observers, corresponding to the two simultaneous tangents to the observers circles. From a geometrical point of view the degeneracy follows from that we can not establish whether the observers lie both “above” or “below” the lens trajectory (Figure 1, top panels). Analytically, the key point is the freedom left by the independence of  $\tau$  from  $u_0$  and  $t_0$  (and  $t_E$ ). Once fixed  $\chi$  according to Eq. 3 we can, independently, fix  $u_0$  so that the trajectory is indeed tangent to the two observers circles, so to recover the observable values  $u_{0,1}$  and  $u_{0,2}$ , and, furthermore, suitably shift  $t_0$  so to get the same observable times at maximum magnification (for a given value of the timescale). Finally, we note that following the habit, we consider the observer impact parameters as signed quantities, although, as geometrically they express a distance, they are intrinsically positive. The sign indicates whether the observer position at maximum magnification lies in the same semi-plane set by the lens trajectory as the origin, or not (the sign being then conventionally positive or negative, respectively), defining a kind of “parity” for the configuration.

The configuration for the two top panels in Figure 1, with the observers lying both in



the same semiplane with respect to the lens trajectory (which in principle can be the same or not as that as the observer in the origin) is said  $\pi_E = \pi_{E,-}$ , with the subscript  $-$  to indicate that in Eq. 2 we take the difference of the impact parameters.

Given the same values for the observer impact parameters and  $\tau$ , from Eq. 2 we can then evaluate a second value for the parallax amplitude,  $\pi_E = \pi_{E,+}$ , taking now the sum of the observers impact parameters. This case corresponds to the geometry configurations shown in Figure 1, bottom panels, with the observers now lying on the opposite sides of the lens trajectory. The new directions for the lens trajectories can be determined by Eq. 3 for which again we can find suitable values of  $u_0$  and  $t_0$  to reproduce exactly the same observed light curves. This completes the four-fold parallax degeneracy for observers at rest. The geometry for the same couple of  $u_{0,1}$  and  $u_{0,2}$  is fixed by  $\pi_E$  (two possible values),  $\chi$  and  $u_0$  (for possible values, each), regardless of the event timescale. Given the geometry, the event timescale fixes the observed difference of the times at maximum magnification.

As a technical point, we note that whereas Eq. 3 can be used only to determine the directions of the lens trajectories, the full equations, namely including  $u_0$ , can be obtained from a geometrical analysis looking for the simultaneous tangents to the two observers circles with the constraint that the distance from the two tangent points must remain equal to  $\tau$ . This way, through simple algebra, we can fully analytically recover the parameters of the 4 degenerate underlying microlensing events giving rise to the observed light curves.

In Figure 2, top panel, we show the light curves corresponding to the four degenerate configurations shown in Figure 1. In the middle and bottom panels we fix the configuration to the four underlying degenerate microlensing events (therefore for appropriate different values for  $u_0$  and  $t_0$ ) and let the angle  $\chi$  vary. For each given configuration we show the variation for  $\Delta t_0$ , middle panel (Eq. 3), and, bottom panels, for the observers impact parameters,  $u_{0,1}$  and  $u_{0,2}$ . In particular  $u_{0,2}$  moves also to negative values, whereas  $u_{0,1}$  remains at the same time positive, corresponding to the configuration with the two observers lying on opposite side with respect to the lens trajectory (which is indeed always the case for the  $\pi_{E,+}$  configurations). The dotted vertical lines indicates the values of the angle  $\chi$  corresponding to the degenerate configurations. We note finally that for each configuration there are two values of  $\chi$  for which we get the same value for  $\Delta t_0$ , but these come with different values of the impact parameters

For reference, the numerical values that fix the configurations shown in Figures 1 and 2 are as follows. The line of sight, towards the Bulge, is fixed at RA, DEC = 266°.8, −21°.4 (with ecliptic latitude  $\beta = 2.0^\circ$ ), with the source, as hereafter we are always going to assume, in the Bulge at  $D_s = 8$ . kpc. We fix (arbitrarily) the observer positions at the Earth and *Spitzer* positions along their orbits (discussed in Section 2.2) at  $t = (\text{JD} - 2450000) =$

6836.0 (June 27, 2014). The four underlying degenerate microlensing event configurations, for timescale  $t_E = 24$  d have parameters (top to bottom, left to right in Figure 1)  $t_0 = (\text{JD} - 2450000) = 6836.0, 6835.17, 6834.73, 6836.45$ ,  $u_0 = 0.80, 0.82, 0.75, 0.73$ , and  $\chi = 30.0^\circ, -24.9^\circ, -11.5^\circ, 16.6^\circ$ ; the two parallax amplitude values are  $\pi_{E,-} = 0.60$  and  $\pi_{E,+} = 1.14$ . The corresponding observers parameters are  $u_{0,(1,2)} = 0.87$  and  $0.30$  with  $t_{0,(1,2)} = 6836.36$  and  $6829.30$  resulting in  $\Delta t_0 = -7.1$  d. The “sign” of  $u_{0,1}$  is always positive, that of  $u_{0,2}$  is negative for two  $\pi_E$  configurations (bottom panels in Figure 1).

Finally, note that in Figure 1 we also indicate the direction of motion. With  $\Delta t_0 < 0$  it results, according to our sign convention,  $t_E > 0$  in the top left and the bottom right panels,  $t_E < 0$  in the others.

## 2.2. Observers in relative motion

We now consider the situation for observers in motion. The case of a single observer, specifically the effect of the Earth orbital motion leading to a deviation from the Paczyński shape and its relationship with the microlensing parallax is known (Gould 1992). The first measure of a microlensing parallax due to this effect was reported by the MACHO collaboration (Alcock et al. 1995) to which many additional cases followed whose physical interpretation is not, however, always straightforward (Poindexter et al. 2005). Moreover (and we recall that we are only discussing single-lens systems), the orbital parallax effect becomes observationally relevant only for a minority of unusually long timescale events. For theoretical analyses of this effect we also refer to Dominik (1998); Smith et al. (2003); Gould (2004). Here our goal is to develop the analysis for two observers in motion within the same framework established in Section 2.1. In particular this will lead us to write a generalization of Eq. 2, and Eq. 3, relevant for this case.

Within the heliocentric frame the lens trajectory is always a straight line. The motion of the observer is taken into account by projecting onto the lens plane the temporal evolution of his (known) orbital motion in the ecliptic plane. Fixed the line of sight, this projection then only depends on the microlensing parallax, with a circular orbit being generically projected into an ellipse. In particular the microlensing parallax is equal to the semimajor axis of the ellipse obtained by projection of the observer orbit on the lens plane.

The microlensing light curve is determined by the temporal evolution of the lens-observer relative projected distance,  $u(t)$ , according to the same expression of the magnification  $A(t) = A(u(t))$  as in Eq. 1 where we have now, however, to take into account of the temporal evolution of the observer position. The combined effect of the two clocks in the system, the

unknown microlensing timescale which fixes the velocity of the lens and the known observer orbital motion, makes that the resulting light curve will no longer be symmetric around the time at maximum magnification. It is still useful, however, to analyse the configuration in terms of the circle centered on the observer position at the time at maximum magnification with radius given by the impact parameter. The specific characteristic for an observer in motion is that this circle is no longer tangent to the lens trajectory, rather, secant. Namely, the key point marking out the difference with respect to the case of an observer at rest is that the impact parameter in general does not coincide with the minimum geometrical distance from the observer projected orbital position at the time at maximum magnification to the lens trajectory.

Let us consider two observers in motion. According to the values of the underlying microlensing event, and specifically of the microlensing parallax, we can still find any of the configurations considered in Section 2.1 and shown in Figure 1 as for the relative position of the observers at the time at maximum magnification with respect to the lens trajectory. Additionally, the relative position of the observers still scales with the microlensing parallax. Accordingly, we can write down an expression similar to Eq. 2 where we have now, however, to take into account the effect of the observers motion

$$\begin{aligned}\vec{\pi}_{E,\pm} &= \frac{\text{AU}}{D_{\perp}} \left( \tau - \Delta u_{0,\parallel}, |u_{0,2,\perp}| \pm |u_{0,1,\perp}| \right), \\ \Delta u_{0,\parallel} &= u_{0,2,\parallel} - u_{0,1,\parallel} \\ u_{0,\text{oss},\parallel} &= |u_{0,\text{oss}}| \sin(\gamma_{\text{oss}}), \quad u_{0,\text{oss},\perp} = |u_{0,\text{oss}}| \cos(\gamma_{\text{oss}}), \quad \text{oss} = 1, 2.\end{aligned}\tag{4}$$

We have introduced here the angle  $\gamma_{\text{oss}}$  centered on the observer position at the time at maximum magnification, between the orthogonal to the lens trajectory and the line to the intersection of the lens trajectory with the circle of radius  $u_{0,\text{oss}}$ , so that  $u_{0,\text{oss},\parallel}$  and  $u_{0,\text{oss},\perp}$  are the projections of the observer impact parameter along and orthogonal to the lens trajectory. In our sign convention, for  $t_E > 0$  according to the discussion in Section 2.1,  $\gamma_{\text{oss}}$  takes negative (positive) values when  $t_{0,\text{oss}}$ , the crossing time of the lens trajectory with the observer circle, comes before (after) the time at the intersection between the lens trajectory and the orthogonal from the circle center. The sign of  $\gamma_{\text{oss}}$  is then reversed for  $t_E < 0$ . This way  $\gamma_{\text{oss}}$ , independently of the direction of the lens motion, therefore of the sign of  $t_E$ , always increases anti-clockwise when looking at the lens plane.

Eq. 4 reduces to that for the case of observers at rest for  $\gamma_{\text{oss}} = 0$ , namely when the lens trajectory is tangent, and not secant as in this case, to the circle centered on the observer position with radius  $u_{0,\text{oss}}$ . Note that the  $\gamma_{\text{oss}}$  are not additional free parameters of the problem, rather, they are determined by the interplay within the lens and the orbital motions. As for Eq. 2, the components of the parallax vector are meant to be written in a

frame with the  $x$ -axis parallel to the lens trajectory. Specifically, as for the case of observers at rest, the microlensing parallax is obtained by application of the Pythagoras theorem. The difference comes because  $\tau$  is (by definition) still equal to the (signed) distance along the lens trajectory between the points of intersection with the observers circles at the time at maximum magnification, so that the  $u_{0,\text{oss},\parallel}$  terms are needed to complete the cathetus delimited by the intersections to the orthogonals from the observer positions to the lens trajectory (in modulus, they can be added or subtracted depending on the sign of  $\gamma_{\text{oss}}$ ).

A key point to be stressed for Eq. 4 is that the notation  $\pm$  for  $\pi_{\text{E},\pm}$  is only meant to describe the two configurations with observers on the same (–) or on opposite (+) sides of the lens trajectory. Because of the observers motion these are however no longer degenerate configurations.

Interestingly, in agreement with Eq. 4, it is possible to write an equation relating the relevant lengths along the lens trajectory analogous of Eq. 3

$$\tau - \Delta u_{0,\parallel} = \pi_{\text{E}} (\cos(\chi)\Delta y_0 - \sin(\chi)\Delta x_0) . \quad (5)$$

Comparing to the case for observers at rest, on the left-hand side the difference, the new term  $\Delta u_{0,\parallel}$ , follows from the appearance of the angles  $\gamma_{\text{oss}}$ ; a key difference is however also found in the right-hand side, although formally identical. Indeed now  $\Delta x_0$ ,  $\Delta y_0$ , the relative observer positions at the time at maximum magnification, are no longer constant (once given the orbit of the observer), rather they depend from all the parameters of the underlying microlensing event configuration, in particular also from  $\chi$ , and indeed the same holds also for the term  $\tau$ . This equation therefore no longer identifies degenerate configurations. The underlying motivation is that, as discussed, the observed light curves, fixed the geometrical configuration, depend from the relative lens-observer motion. Any variation in the microlensing parameters is then reflected, in particular, in a change of the observer positions at the time at maximum magnification and ultimately in the light curve observables. In principle, one can invert this line of thought and claim that there is a relationship between the observables, impact parameter and time at maximum magnification, and in particular the timescale of the underlying microlensing event.

### 3. Analysis

In the previous sections we have revisited the underlying geometrical and mathematical foundations for the description of the measure of the microlens parallax from two distant observers. In particular we have put in evidence the differences which arises moving from the case of observers at rest to that of observers in relative motion writing down an extension of

the Gould (1994) parallax equation valid for observers at rest to this case. In this Section first we show an example of the configuration described in Section 2.2 then we highlight, through specific examples, the importance of fully taking into account the relative motion of the observers for a correct understanding of the underlying microlensing parallax signal.

As above, for definiteness we consider the case of the simultaneous observation of the same microlensing event from ground and from *Spitzer*. *Spitzer* (Werner et al. 2004) moves along an heliocentric, “earth-trailing”, orbit, currently at a distance of about 1 AU from Earth<sup>3</sup>. For simplicity of the discussion but still accurately enough, we approximate both Earth’s and *Spitzer*’s orbits as circular, with radius 1 AU and constant angular velocity with a period of 1 year and 373 d, respectively. We fix the Earth and *Spitzer* phases, their relative azimuthal angles, at the time of the autumnal equinox. For 2014, at  $\text{JD} - 2450000 = 6923.6$ ,  $\Delta\lambda = -79.7^\circ$ .

In Figure 3 we show a specific two-observers microlensing parallax configuration on the lens plane. The analysis is carried out following the discussion in Section 2.2. In particular, we evaluate the observers impact parameters and time at maximum magnifications through a numerical minimization of the function  $u(t)$  taking into account both the lens and the observers orbital motion. The ellipse indicates the projection of the Earth, and *Spitzer*, orbit on the lens plane. The dotted points along the trajectories are equally spaced by 5 d, with empty symbols for times prior  $t_0$ , showing the direction of motion. We remark, as discussed in Section 2.2, that the lens trajectory is *secant* to the two circles of radius  $u_{0,\text{oss}}$  centered on the orbital positions at time  $t_{0,\text{oss}}$  (and no longer tangent as for the case of observers at rest, Figure 1). For reference, the microlensing event configuration is as follows. The line of sight, towards the Bulge, is fixed at  $\text{RA}, \text{DEC} = 266^\circ.8, -21^\circ.4$  (we see here a generic feature of the *Spitzer* observational campaign in 2014 and 2015, with Earth and *Spitzer* almost aligned along the equatorial axis). The microlensing event parameters are  $t_0 = (\text{JD} - 2450000) = 6836.0$ ,  $u_0 = 0.4$ ,  $t_E = 28.5$  d,  $\chi = 45^\circ$  and  $\pi_E = 0.76$  which results into a  $\pi_{E,+}$  configuration, observers on different sides of the lens trajectory with  $u_{0,(1,2)} = 0.47, 0.15$  and  $t_{0,(1,2)} = 6831.5, 6821.2$  with  $\Delta t_0 = -10.3$  d. Comparing to the case of observers at rest there is now, in agreement with Eq. 4, a non-zero value for  $\gamma_{\text{oss}}$  with  $\gamma_{1,2} = -20^\circ$  and  $2^\circ$  (note in particular the negative sign of  $\gamma_1$ ). As further detailed below, it is useful to estimate a proxy for the event timescale analog to the Einstein time for the observed light curves. In this case it results  $t_{e,\text{oss}}$  equal to 36 and 29 days, respectively.

In Figure 4 we show, top panel, the light curves for the microlensing event shown in

---

<sup>3</sup>The ephemeris of *Spitzer* as a function of time can be found on the NASA-JPL Horizon system <http://ssd.jpl.nasa.gov/?horizons>.

Figure 3 as would be seen from the Sun, and those for the Earth and *Spitzer* observers. In the middle and bottom panels we show a few characteristics quantities for this microlensing event configuration by varying the angle  $\chi$ . In particular, we show  $\Delta t_0$  and  $u_{0,\text{oss}}$ , no longer symmetric as in the case with observers at rest (Figure 1). Furthermore, we show the characteristics quantities for observers in motion: the angle  $\gamma_{\text{oss}}$ , which we see can become rather large, and the estimated timescale along the observers light curves,  $t_{\text{E,oss}}$ . Note that, besides  $u_{0,\text{oss}}$ , also  $\gamma_{\text{oss}}$  is shown taking into account the sign of the configuration as defined in Section 2.1. The inspection of the bottom-right panel reveals that the  $t_{\text{E,oss}}$  values can get to be significantly different one from the other, and from the duration of the underlying microlensing event,  $t_{\text{E}}$ . Indeed, also comparing to Figure 3, we see that the larger differences for  $t_{\text{E},1}$  from  $t_{\text{E}}$  occurs for a lens direction of motion about along the  $x$  axis. This is so because of the Earth position along its orbit at the time at maximum magnification, with the relative lens-observer velocity getting to a minimum (maximum), and correspondingly the duration a maximum (minimum) for values about  $\chi = \pi/2$  ( $3\pi/2$ ) respectively<sup>4</sup>.

In Section 2.2 we have discussed the underlying reason why the microlensing parallax degeneracy is broken once introduced the observer motion. One may however assume that the deviations from the case with observers at rest are in some sense “small” and look also in this case for the analog of the degenerate configurations discussed with observers at rest. More specifically, the ratio of the analysis is the following. For a given set of parameters we evaluate, following the analysis in Section 2.2, the microlensing light curves as seen by the observers in motion, and in particular the values for the impact parameter and time at maximum magnification,  $(u_0, t_0)_{\text{oss}}$ . We then consider as given these values, fix the positions of the observers along their orbits at their respective time at maximum magnification and, following the analysis in Section 2.1, study the event under the assumption of observers at rest, namely through Eq. 2 and Eq. 3. In particular we can evaluate and compare the resulting values for the degenerate solutions of the microlensing parallax to the “true” value.

Additionally, we consider the observed timescale, key to address the issue of the breaking of the parallax degeneracy. Indeed, Gould (1995) acknowledged that the microlensing parallax fourfold degeneracy is broken as soon as one drops the assumption of observers at rest and in particular remarked that the two observers (from ground and from the satellite) would measure a different timescale. Gould (1995) then derived a relationship (his Eq. 2.3) for evaluating the difference of the observed parameters given the relative motion of the observers, and all in principle directly observables quantities: the timescale difference (rather,  $\Delta\omega$ , the difference of the inverse of the timescale,  $\omega = 1/t_{\text{E}}$ ), and the difference of the times

---

<sup>4</sup>Our sign convention for  $t_{\text{E}}$ , as also apparent from Figure 3, is the same as in Section 2.1.

at maximum magnification. This same equation was then the basis to address the issue of the possibility of breaking the degeneracy for the analyses by Bouteux & Gould (1996) and Gaudi & Gould (1997) with the simulation of parallax microlens events towards the Magellanic Clouds and the Galactic bulge, respectively.

From the standpoint of our analysis in Section 2.2, considering in particular Eq. 4, it is however relevant to observe that the analysis in Gould (1995) is still based on Eq. 2 valid for the case of observers at rest. Looking at the relationship obtained by Gould (1995) as an equation for  $\Delta\omega$ , we may therefore compare this “expected” value to the “true” one which we can estimate from the analysis of the light curves. This way we can test whether the estimate is reliable for assessing the breaking of the degeneracy.

Before moving on presenting the results of this analysis we pause to specify what we intend by “timescale” for the case of observers in motion. The Einstein time,  $t_E$ , as it appears in Eq. 1, is well defined for a light curve symmetric around the time at maximum magnification,  $t_0$ , and in particular it results that the magnification  $A(t)$  for  $t = t_E$  is that evaluated for a value  $u(t) = \sqrt{u_0^2 + 1}$ . As detailed above, the light curve for observers in motion is no longer symmetric and by itself a single parameter as the timescale, however defined, can not grasp both the width of the light curve and the degree of asymmetry. Still, it remains a useful indicator of the light curve shape. Based on the definition valid for an observer at rest, as a proxy for the timescale for observers in motion we proceed as follows. Given the observable  $u_{0,\text{oss}}$  we evaluate the value of the magnification of an hypothetical Paczyński light curve with this value for the impact parameter at the time corresponding to that of the Einstein time, which we call  $\bar{A}$ . Moving back to the observed light curve, we numerically evaluate the time interval, in general asymmetric around the time at maximum magnification, fixed by the intersection of the light curve with the value  $\bar{A}$  and define the “Einstein time” for the observer in motion,  $t_{E,\text{oss}}$ , as half this interval (with the true  $t_E$  being therefore recovered for a symmetric light curve).

We fix the line of sight towards the Bulge and  $t_0$  as in Figures 1 and 2. Fixed the lens mass at  $0.6 M_\odot$  we consider two cases: a lens in the disc, at  $D_l = 2.0$  kpc, and a lens in the Bulge, at  $D_l = 7.5$  kpc. This results, always for  $D_s = 8$  kpc, in  $\pi_E = 0.28$  and  $0.04$ , respectively. For  $v = 300$  and  $80$  km/s, the timescale is  $16$  and  $59$  d for the disc lens and  $8.7$  and  $33$  d for the bulge lens. In Figure 5 and 6 (bulge and disc lens, respectively) we show for two values of the impact parameter,  $u_0 = 0.1$  and  $0.8$  (from top to bottom, for increasing impact parameter and event duration), as a function of the angle of the lens motion  $\chi$ , the values for  $u_{0,\text{oss}}$ , the horizontal solid line indicates  $u_0$  for the Sun observer, those for  $\pi_{E,\Delta\pm}$  as calculated for observers at rest, where the solid horizontal line indicates the true value for  $\pi_E$ , and  $\Delta\omega$  corresponding to  $\pi_{E,\Delta\pm}$ . Note that the two degenerate solutions

for the parallax amplitude, and correspondingly the values for  $\Delta\omega$ , are evaluated based on  $\Delta_{\pm} \equiv \Delta u_{0,\pm} = u_{0,2} \pm u_{0,1}$ , namely taking into account the sign of  $u_{0,\text{oss}}$ . This way the  $\Delta_-$  solution has always the same parity of the original configuration,  $\pi_{E,-}$  or  $\pi_{E,+}$  (with the changes between the parity following the sign of  $u_{0,\text{oss}}$ ). Indeed we can see that the  $\pi_{E,\Delta-}$  solution remains always close enough to the true value, whereas  $\pi_{E,\Delta+}$  can get quite different. Interestingly, however, there are also ranges of  $\chi$  values for which  $\pi_{E,\Delta+}$  can get closer to the true value than  $\pi_{E,\Delta-}$ , so that in principle the analysis based on the assumption of observers at rest may lead to the correct value for  $\pi_E$  although with the wrong sign of the parity. In general we see that a larger value of  $u_0$  or  $t_E$  makes both the difference between the  $\pi_{E,\Delta-}$  and  $\pi_{E,\Delta+}$  values and the relative difference with respect to the true value  $\pi_E$  larger, as well as it makes larger the difference between  $\Delta\omega$  calculated for observers at rest with respect to the true value. However, whereas for the bulge lens these differences do not ever become really significant, so that the lens motion may indeed be neglected in the analysis, this is no longer true for the disc lens configuration. It is apparent, therefore, that, besides the effect of the direction of motion, larger values of the microlens parallax (for large enough  $u_0$ ), therefore for decreasing values of the lens mass and nearer lenses, tend to enhance the importance of the observers motion. This effect is however balanced by the event duration which on the other hand decreases both with the lens mass and the lens distance.

#### 4. K2 and *Spitzer* parallax: a 3 observers problem

K2 (Howell et al. 2014), the extension of the *Kepler* (Borucki et al. 2010; Koch et al. 2010) mission, is expected to carry out in spring 2016 a three months microlensing monitoring towards the Galactic bulge during its K2C9 campaign, the first space-based microlensing survey ever (Henderson et al. 2015). The K2 survey mode of operation is opposed to that of the *Spitzer* observational program which monitors microlensing events in a follow-up mode (Yee et al. 2015a). This will allow K2 to address several relevant scientific questions related to the observation of a typology of microlensing events, such as high magnification and/or short timescale ones, which are likely to be missed by *Spitzer*.

*Kepler* is moving along an Earth-trailing orbit similar to that of *Spitzer* which therefore we approximate in a similar way as in Section 2.2 (the exact ephemeris can be found on the NASA-JPL Horizon system). We fix the phase shifts at the fall equinox 2016,  $\text{JD} - 2450000 = 7654.1$ , for *Spitzer* and K2 at  $\Delta\lambda = -94^\circ.4, -52^\circ.7$ , respectively.

K2C9 is going to last about three months, starting April 2016, so that this observational period will (partly) overlap with that of the expected 2016 *Spitzer* follow-up microlensing project expected to start in June 2016 (we recall that this campaign must obey the *Spitzer*



visibility constraints towards the Bulge). For the first time it is going to be possible to observe simultaneously the same microlensing events from ground and two satellites in orbit. This is relevant to our analysis because, already within the framework of observers at rest, the fourfold degeneracy is broken by the introduction of a third observer, an effect enhanced when correctly taking into account the motion of the observers. It is however interesting to address this issue within the framework of observers at rest to appreciate to which extent the degeneracy gets actually broken. From the inspection of Eq. 3 we see that the difference between the times at maximum amplification is going to be different for K2 and *Spitzer*, so that the respective degenerate solutions for the lens trajectory are going to be different. Eq. 2 then implies that the difference in the impact parameters will then determine two different sets of  $\pi_{E,\pm}$  solutions, giving therefore the chance, when analysed together, to single out the correct one (we recall that the degeneracy breaking for K2 microlens parallaxes is the specific purpose of one of the accepted proposals (Gould et al. 2015a) for the forecoming 2016 *Spitzer* campaign).

This is exemplified in Figure 7 where we show the configuration in the lens plane for the three observers case for a specific microlensing event configuration and 4 test values of the lens trajectory. We show the circles of radius  $u_{0,\text{oss}}$  centered on the observers positions (here considered at rest, as evaluated at  $t = t_0$ ) and the lens trajectory which is now simultaneously tangent to all three observer circles. At glance it is clear that, when considering both the couples of observers simultaneously, the degeneracy for the parallax vector directions and amplitude is broken. For reference, we fix the line of sight to that expected to be the center of K2C9 field, RA, DEC =  $270^\circ.354$ ,  $-21^\circ.780$ . We fix  $t_0 = (\text{JD} - 2450000) = 7561$  (June 21, 2016),  $u_0 = 0.5$ ,  $t_E = 24$  d,  $\pi_E = 0.8$  and test 4 values for the angle of the lens trajectory (top to bottom, left to right)  $\chi = 15^\circ$ ,  $30^\circ$ ,  $45^\circ$  and  $60^\circ$ . The resulting  $u_0$  from ground is always about 0.52 – 0.53, for *Spitzer* 0.28, 0.20, 0.078 and 0.084 and for K2 0.087, 0.025, 0.073 and 0.2;  $\Delta t_0$  is -4.0, -8.8, -13., -16. days for *Spitzer* and -3.3, -7.0, -10 and -13 days for K2, respectively. The degenerate directions, for each couple Earth-*Spitzer* and Earth-K2 are clearly different. The resulting degenerate values of the parallax amplitude are different as well. In particular (for a true value  $\pi_E = 0.8$ ) for *Spitzer* and K2 we evaluate 0.29 and 0.59 ( $\chi = 15^\circ$ ), 0.48 and 0.74 ( $\chi = 30^\circ$ ), 0.69 and 0.94 ( $\chi = 45^\circ$ ) and 0.90 and 1.15 ( $\chi = 60^\circ$ ), so that for this configuration the degenerate solution shifts from  $\pi_{E,-}$  to  $\pi_{E,+}$  at  $\chi = 45^\circ$  for K2 and at  $\chi = 60^\circ$  for *Spitzer*. Clearly, the degree by which the degeneracy is broken can be measured by how much the degenerate solutions, in term of direction or of the amplitude of  $\vec{\pi}_E$ , differ one from the other when considering simultaneously the two couples of observers. Hereafter we are going to focus on the amplitude of the microlensing parallax.

For the analysis of Figure 7 we have considered the respective positions of the observers along their orbit, specifically given their (fixed) phase shift. This is indeed a relevant aspect

which leads us to discuss the seasonal effects for the measure of the microlens parallax for two observers lying both along the ecliptic plane. Indeed, the line of sight towards the Bulge is near the ecliptic plane therefore the projection on the lens plane of the distance between the two observers (which remains roughly constant on the ecliptic plane along the few months of a given observation campaign) is a strong function of the period of the year. This is relevant because, from Eq. 2, we see that  $\pi_E \propto 1/D_\perp$ . All the microlensing parameters fixed, in particular the parallax, whenever  $D_\perp$  becomes very small, namely when the two observers are roughly aligned with the line of sight towards the Bulge, the larger we can expect the degenerate parallax solution to be. On the other hand,  $\pi_E \propto \sqrt{1/M_l} \sqrt{(1-x)/x}$ , so that large values for  $\pi_E$  are expected for very small lens mass or very nearby lenses. Too extreme values (at least for lenses in the stellar mass range), roughly  $\pi_E > 2$ , are however by themselves extremely unlikely.

In Figure 8 we show the variation of the degenerate parallax solution,  $\pi_{E,2}$  (which can be  $\pi_{E,-}$  or  $\pi_{E,+}$ ) as a function of the time of the year,  $\bar{t}$ . Specifically, we fix the underlying microlensing event configurations with in particular the time at maximum magnification, as seen from the ideal observer on the Sun, at  $t_0 = \bar{t}$ . At the same time we fix the positions along the orbit of the three observers, Earth, *Spitzer* and K2, at  $t_0 = \bar{t}$ . In particular, given the line of sight, the direction of the lens motion and the event timescale, we show the results for different combinations of the impact parameter and the microlens parallax. For reference, the line of sight is fixed as for the events shown in Figure 7,  $t_E = 24$  d and  $\chi = 30^\circ$ . We then test two values for the microlens parallax,  $\pi_E = 0.01$  (two top panels) and  $\pi_E = 1.3$  and two values for the impact parameter,  $u_0 = 0.01$  (top to bottom, first and third panels =) and  $u_0 = 0.8$ . At glance we can see that the difference in the orbital phase shift between *Spitzer* and K2 introduces a shift in the peak for  $\pi_{E,2}$  and that, besides  $\bar{t}$ , also the underlying microlensing configuration plays a relevant role leading even to rather wild variations. Focusing in particular on June 2016, starting about JD-2450000=7550, when the *Spitzer* and K2 campaigns will overlap, we see that, quite regardless of the microlens parallax value, small values for the impact parameter tend to smooth over the difference between the  $\pi_{E,2}$  values as seen by *Spitzer* and K2, whereas larger values for  $u_0$  lead quickly to a rather large offset between the two  $\pi_{E,2}$  values which can therefore resolve the parallax degeneracy. Finally, we note that for *Spitzer*, within the boundaries of the observational window,  $\pi_{E,2}$  tend to remain always roughly constant, or in any case bounded to smaller value, which is not the case, however, for K2.

## 5. Conclusion

In this work we have revisited the analysis of the microlensing parallax for the case of the simultaneous observation of the same microlensing event by two, and three, observers (Refsdal 1966; Gould 1994) from within an heliocentric frame. The main purpose of this analysis is the understanding of the fourfold microlensing parallax degeneracy and of how it is broken. First we have discussed the case for observers at rest and went through the geometrical meaning of the microlensing parallax degeneracy, in particular we have explicitly written down an expression for the degenerate directions of the lens trajectory as a function of the microlensing parallax,  $\pi_E$ , and  $\tau = \Delta t_0/t_E$  only. Second, we have considered the case for observers in motion and we have written down an extension to this case of the Gould (1994) relationship between the microlensing parallax and the light curve observables. We have discussed how the geometry of the microlensing parallax configuration is now determined by all the parameters of the underlying microlensing event, in particular the duration, which is the underlying reason for the breaking of the degeneracy in this case. Through all the analysis, the choice of an heliocentric reference frame allowed us to get a clear geometrical and analytical insight.

As test case we have considered simultaneous observations from ground and *Spitzer*, relevant in consideration of the ongoing follow-up observational campaign towards the Galactic Bulge (Gould et al. 2013, 2014, 2015a,b). The analysis, through a series of test cases, hints that the motion of the observers can be expected to be relevant especially for disc lenses with large enough impact parameters and long enough timescale. These are the cases, therefore, for which one may expect to be able to break more easily the degeneracy also from an observational point of view.

Finally, we have discussed the case for three simultaneous observers, relevant for the foreseen K2 microlensing survey expected for 2016, which will also partly overlap with the *Spitzer* season. The microlensing parallax degeneracy is there broken already from the standpoint of an analysis based on the assumption of observers at rest. Through a series of test cases we have shown how this can be actually effective.

In this work we explicitly have not addressed the issue of the actual determination of the microlensing parameters out of observed light curves. We recall that as a standard, for instance for the analysis of the *Spitzer* light curves (Calchi Novati et al. 2015a) the scheme developed by Gould (2004) from within a geocentric frame is used. A drawback of this approach is that in the end one has to come back to the heliocentric frame for the determination of some parameters, notably the event duration. A main advantage, however, is that the observed underlying event parameters, time of maximum magnification, impact parameter and duration, are similar to those which can be estimated from ground in absence of the

parallax effect. In principle, though, this is exactly where the simultaneous observation from a space observer may help. With reference to the *Spitzer* campaign, however, we recall that, even put aside the problems related to the determination of the source flux and the different blend fractions, the limited baseline in most cases does not allow to fully independently characterize the microlensing light curve. This represents a major problem for the practical application of the analysis presented in this work, and this holds in particular for the case of the three observatories. Still, it is going to be interesting to analyse the K2 data which, thanks to the survey mode and longer baseline available, may be expected to suffer less from this limitation.

We thank A. Gould for valuable discussions. SCN acknowledges support by JPL grant 1500811. GS thanks NExScI for hospitality at Caltech during part of this work.

## REFERENCES

- Alcock, C., et al. 1995, *ApJ*, 454, L125
- Batista, V., Beaulieu, J.-P., Bennett, D. P., Gould, A., Marquette, J.-B., Fukui, A., & Bhattacharya, A. 2015, *ApJ*, 808, 170
- Bennett, D. P., et al. 2015, *ApJ*, 808, 169
- Borucki, W. J., et al. 2010, *Science*, 327, 977
- Boutreux, T., & Gould, A. 1996, *ApJ*, 462, 705
- Calchi Novati, S., et al. 2015a, *ApJ*, 804, 20
- Calchi Novati, S., et al. 2015b, *ApJ*, 814, 92
- Dominik, M. 1998, *A&A*, 329, 361
- Dong, S., et al. 2007, *ApJ*, 664, 862
- Gaudi, B. S., & Gould, A. 1997, *ApJ*, 477, 152
- Gould, A. 1992, *ApJ*, 392, 442
- Gould, A. 1994, *ApJ*, 421, L75
- Gould, A. 1995, *ApJ*, 441, L21

- Gould, A. 1997, *ApJ*, 480, 188
- Gould, A. 1999, *ApJ*, 514, 869
- Gould, A. 2000, *ApJ*, 542, 785
- Gould, A. 2004, *ApJ*, 606, 319
- Gould, A. 2013, *ApJ*, 763, L35
- Gould, A. 2014, *Journal of Korean Astronomical Society*, 47, 215
- Gould, A., Carey, S., & Yee, J. 2013, *Spitzer Microlens Planets and Parallaxes*, *Spitzer Proposal*
- Gould, A., Carey, S., & Yee, J. 2014, *Galactic Distribution of Planets from Spitzer Microlens Parallaxes*, *Spitzer Proposal*
- Gould, A., et al. 2006, *ApJ*, 644, L37
- Gould, A., Yee, J., & Carey, S. 2015a, *Degeneracy Breaking for K2 Microlens Parallaxes*, *Spitzer Proposal*
- Gould, A., Yee, J., & Carey, S. 2015b, *Galactic Distribution of Planets From High-Magnification Microlensing Events*, *Spitzer Proposal*
- Henderson, C. B., et al. 2014, *ApJ*, 794, 71
- Henderson, C. B., et al. 2015, *ArXiv:1512.09142*, *PASP* submitted
- Howell, S. B., et al. 2014, *PASP*, 126, 398
- Koch, D. G., et al. 2010, *ApJ*, 713, L79
- Mao, S. 2012, *Research in Astronomy and Astrophysics*, 12, 947
- Paczynski, B. 1986, *ApJ*, 304, 1
- Penny, M. T., Henderson, C. B., & Clanton, C. 2016, *ArXiv:1601.02807*, *ApJ* submitted
- Poindexter, S., Afonso, C., Bennett, D. P., Glicenstein, J.-F., Gould, A., Szymański, M. K., & Udalski, A. 2005, *ApJ*, 633, 914
- Refsdal, S. 1966, *MNRAS*, 134, 315
- Smith, M. C., Mao, S., & Paczyński, B. 2003, *MNRAS*, 339, 925

- Spergel, D., et al. 2015, ArXiv:1503.03757
- Street, R. A., et al. 2015, ArXiv:1508.07027, ApJ submitted
- Udalski, A., et al. 2015, ApJ, 799, 237
- Werner, M. W., et al. 2004, ApJS, 154, 1
- Yee, J. C. 2013, ApJ, 770, L31
- Yee, J. C., et al. 2015a, ApJ, 810, 155
- Yee, J. C., et al. 2015b, ApJ, 802, 76
- Zhu, W., et al. 2015, ArXiv:1510.02097, ApJ submitted

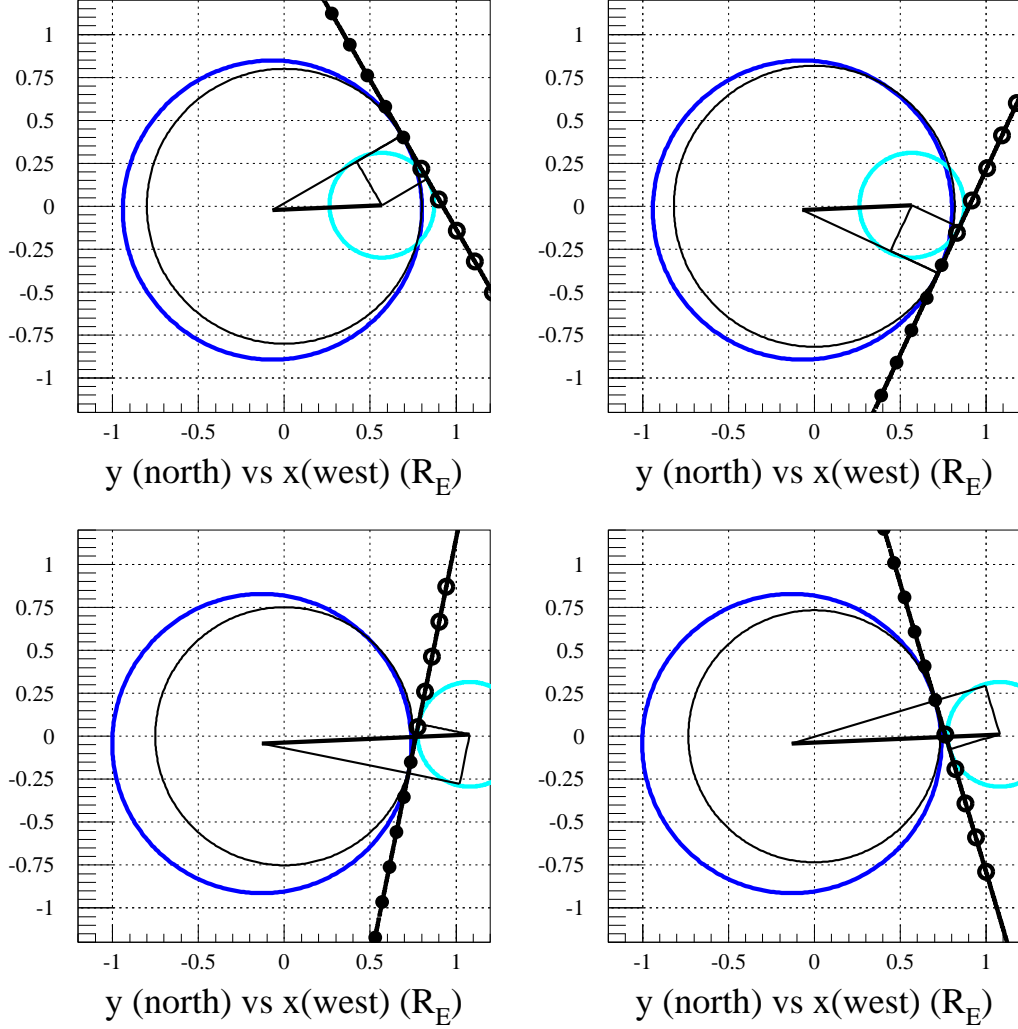


Fig. 1.— Projected in the lens plane, in a heliocentric reference frame centered on the line of sight to the source, the 4 degenerate configurations for the same microlensing light curves as observed by two observers at rest on Earth and *Spitzer* for a line of sight towards the Bulge (see Section 2.1 for full details). Top (bottom) panels for the  $\pi_{E,-}$  ( $\pi_{E,+}$ ) configurations, respectively. The thin black circle is centered on the origin, radius the impact parameter as would be seen from the Sun. The thick circles are centered on the observer positions, with radius the respective impact parameters, dark and light blue for Earth and *Spitzer*. The straight lines simultaneously tangent to the three circles represent the lens trajectory, the dots along it are equally spaced by 5 days, empty ones for times prior  $t_0$ . The centers of the Earth and *Spitzer* circles are joined by a thick line, whose length scales with the microlensing parallax; the thinner lines indicates the triangle construction underlying Eq. 2. The  $x$  and  $y$ -axes are along the equatorial directions (west and north, respectively), the  $z$  axis along the line of sight, as seen from the Sun.

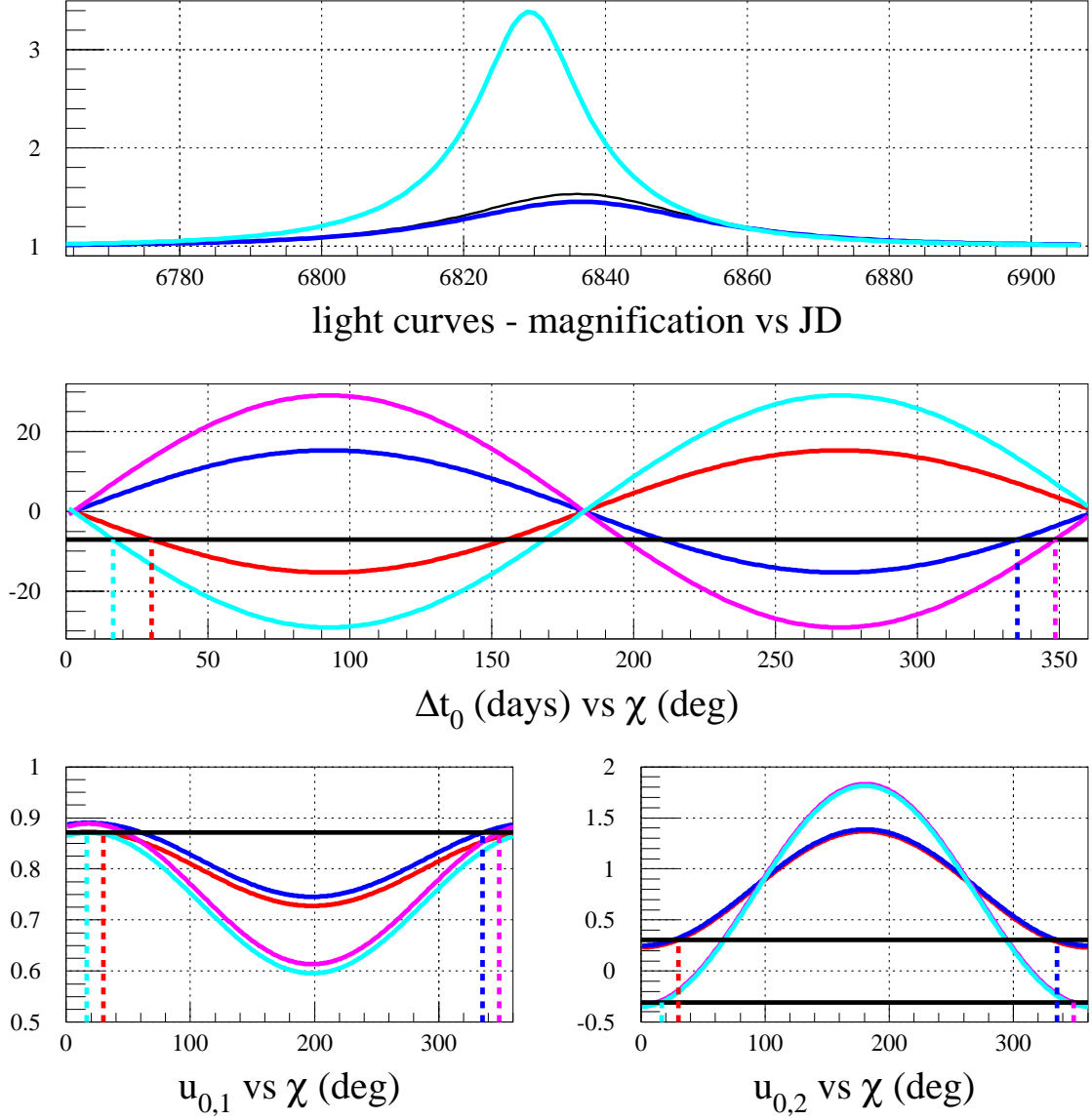


Fig. 2.— Top panel: the light curves corresponding to the event configurations shown in Figure 1. The thin black line for one out of four degenerate solutions as would be seen from the Sun, in dark and light blue the light curves as seen from Earth and from *Spitzer*. Middle and bottom panels: difference of the observers times at maximum magnification,  $\Delta t_0$  (middle panel), and observer impact parameters,  $u_{0(1,2)}$ , for the four degenerate underlying solutions as would be seen from the Sun, as a function of the angle identifying the direction of the lens trajectory,  $\chi$ . The solid horizontal lines indicate the values, for  $\Delta t_0$  and  $u_{0(1,2)}$ , corresponding to the case shown in Figure 1, with the vertical dotted lines marking the values of the corresponding angles  $\chi$ . See Section 2.1 for full details on the event configuration.



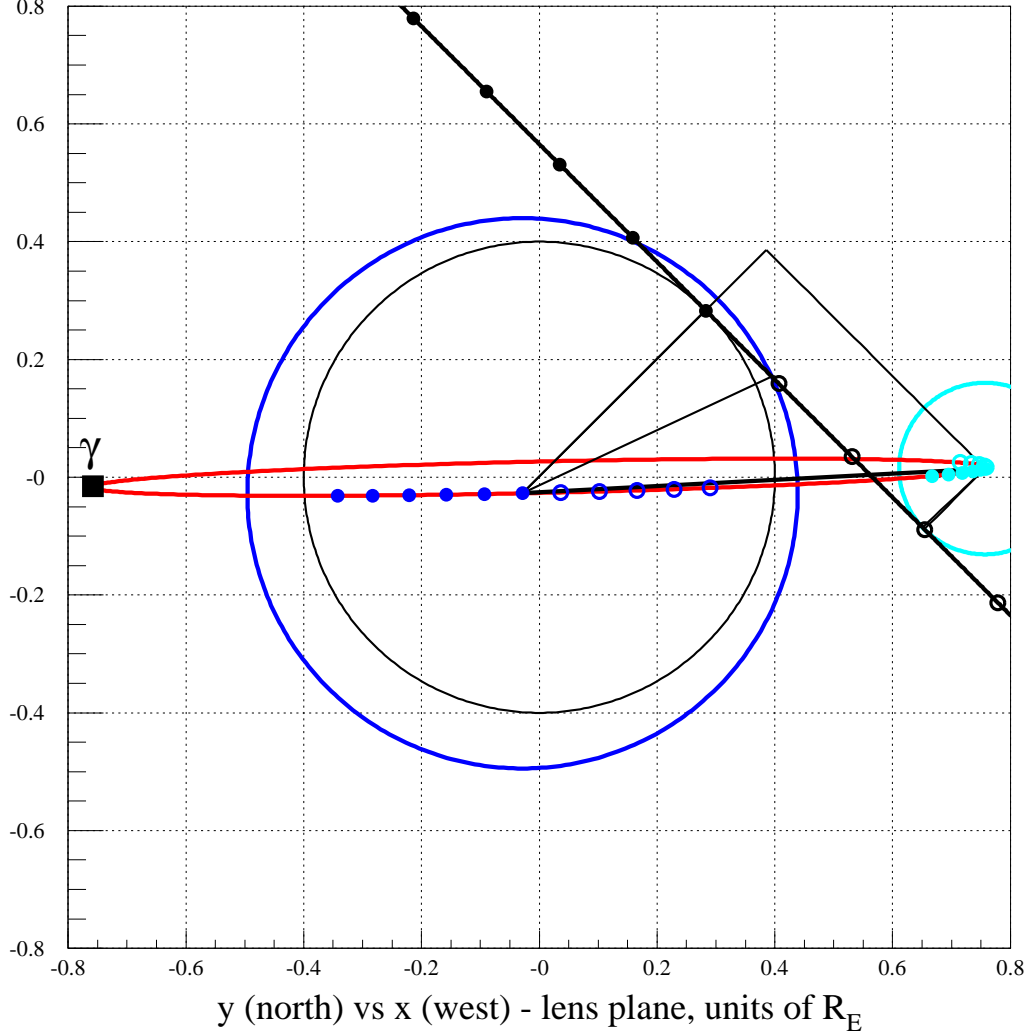


Fig. 3.— Projected in the lens plane, in an heliocentric reference frame centered on the line of sight to the source, the configuration for a parallax microlensing event for two observers in motion, on Earth and *Spitzer*, for a line of sight towards the Bulge (see Section 2.2 for full details). The thin black circle is centered on the origin, radius the impact parameter as would be seen from the Sun. The thick circles are centered on the observer positions at the times of their respective maximum magnification with radius their respective impact parameters, dark and light blue for Earth and *Spitzer*. The red elongated ellipse represents the projected orbit of the observers (the square indicates the position of the Earth at the fall equinox). The thick straight line tangent to the circle of radius  $u_0$ , secant to the observer circles, is the lens trajectory. The dots along the trajectories are equally spaced by 5 days, empty ones for times prior the respective times at maximum magnification. The centers of the Earth and *Spitzer* circles are joined by a thick line, whose length scales with the microlensing parallax, the thinner lines indicates the triangle construction underlying Eq. 4. The reference frame is as in Figure 1.

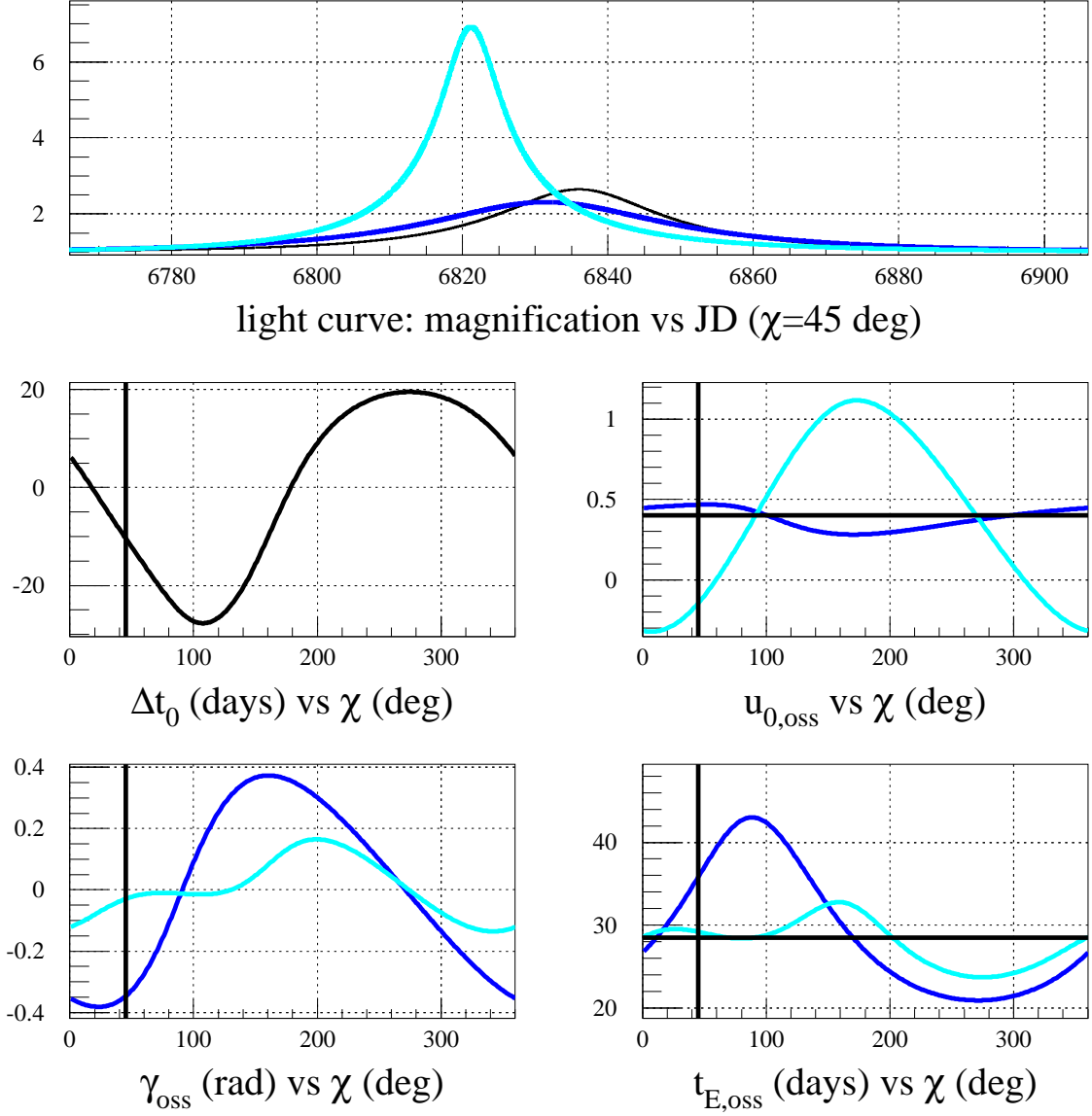


Fig. 4.— Top panel: the light curves for the microlensing event configuration shown in Figure 3. The thin black line for the event as would be seen from the Sun; in dark and light blue the light curves as seen from Earth and from *Spitzer*. Middle and bottom panels: for the same event configuration, varying the angle  $\chi$  of the direction of the lens trajectory, difference of time at maximum magnification,  $\Delta t_0$ , observers impact parameters,  $u_{0,oss}$ , angle  $\gamma_{oss}$  and duration for the observers light curves,  $t_{E,oss}$ . The vertical lines indicate the value for  $\chi$  used for the light curves in the top panel, the horizontal lines the values  $u_0$  and  $t_E$  of the underlying microlensing event as seen from the Sun.

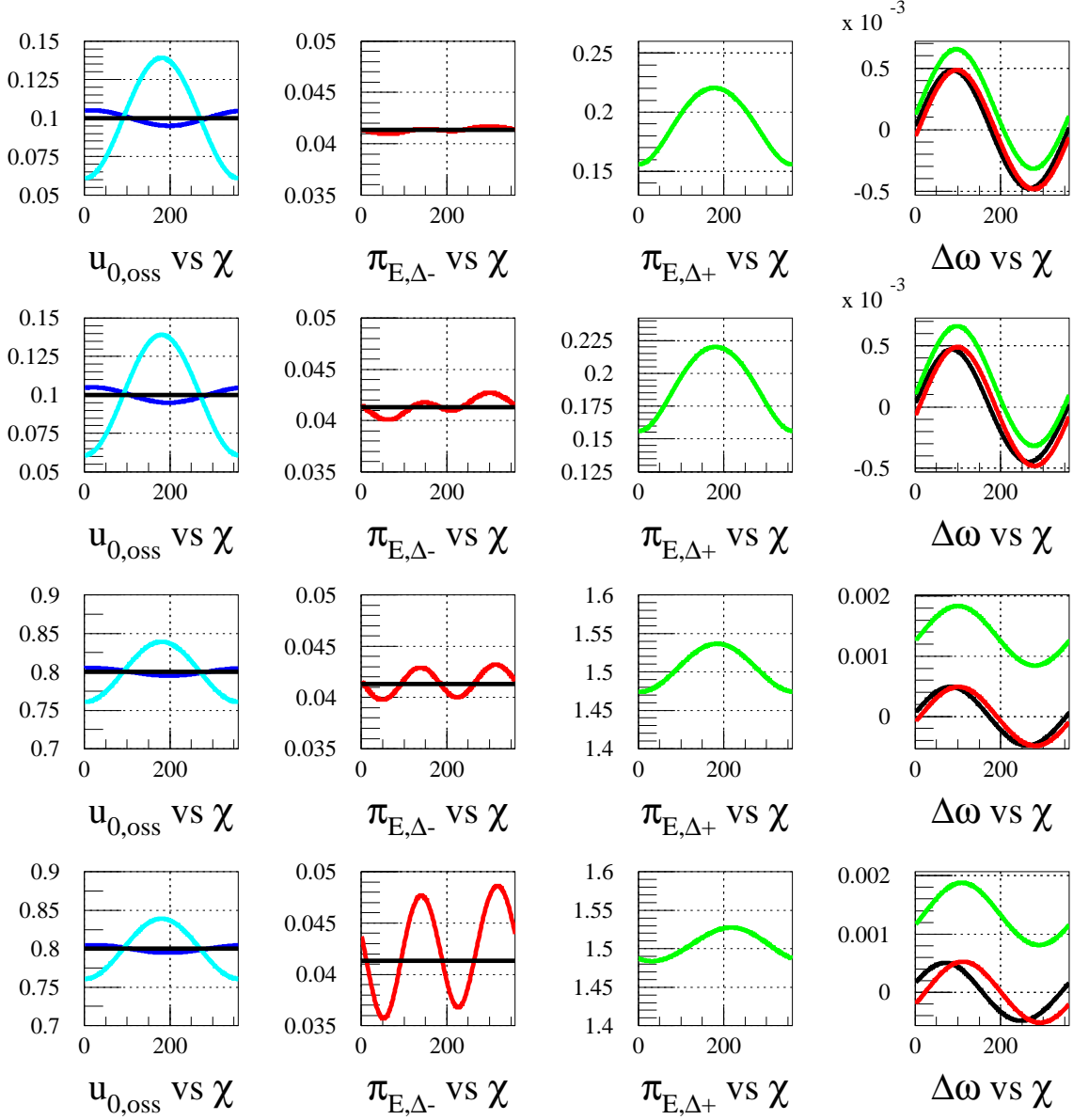


Fig. 5.— For a Bulge lens, as a function of the direction of the the lens trajectory, angle  $\chi$  expressed in degree, we show, from left to right,  $u_{0,oss}$ , as evaluated for observers in motion, and the corresponding values as evaluated assuming observers at rest for  $\pi_{E,\Delta\pm}$  and  $\Delta\omega$ , the true value in black, in red and green those corresponding to  $\pi_{E,\Delta\pm}$ . The solid horizontal lines for  $u_0$  and  $\pi_E$  indicate respectively the impact parameter as would be seen from the Sun and the value of the microlens parallax for the underlying microlensing event. From top to bottom we show different configurations increasing the value of the impact parameter and the event duration. We refer to Section 3 for full details.

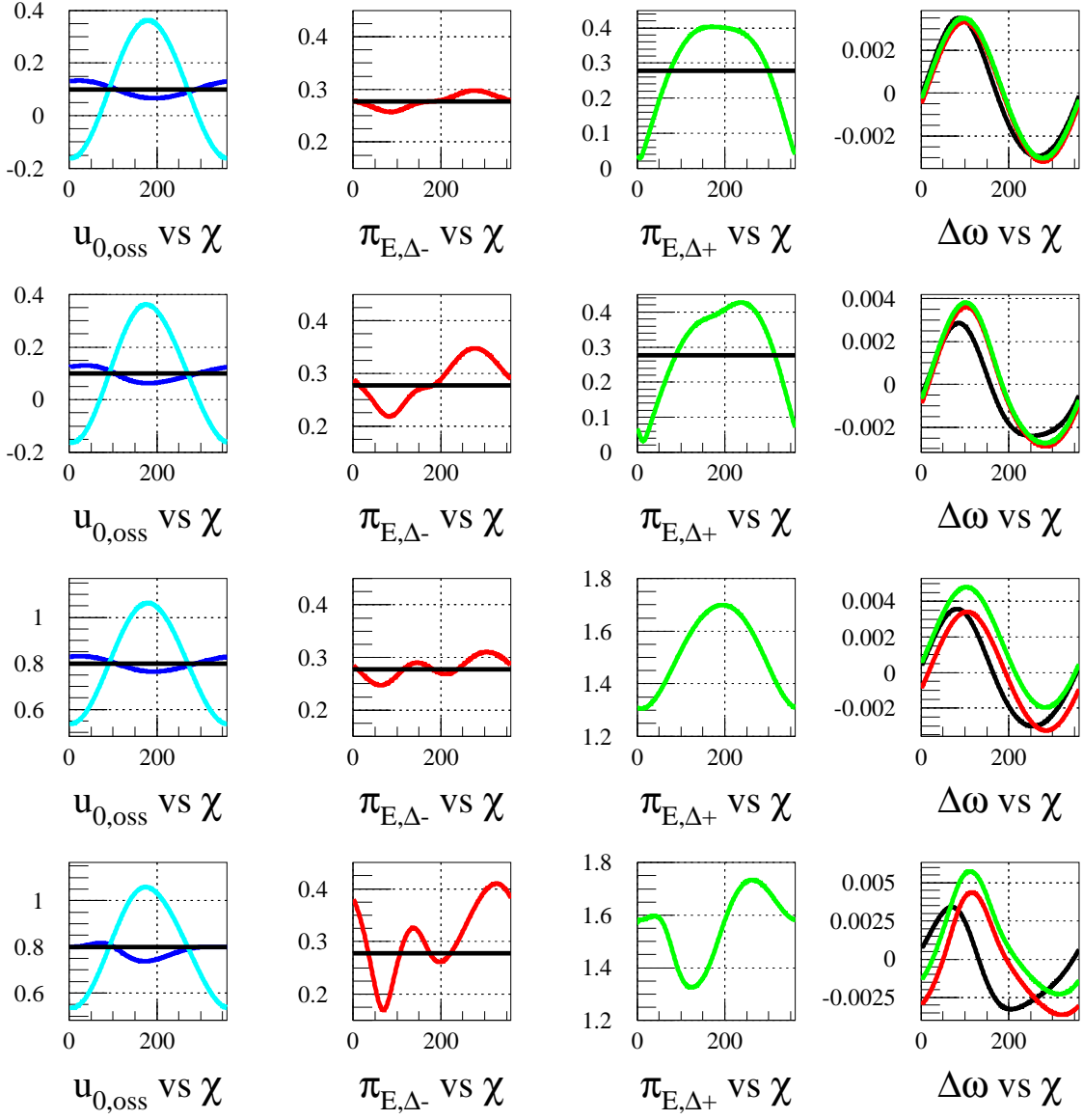


Fig. 6.— The same as in Figure 5, here for a lens in the Disc. We refer to Section 3 for full details.

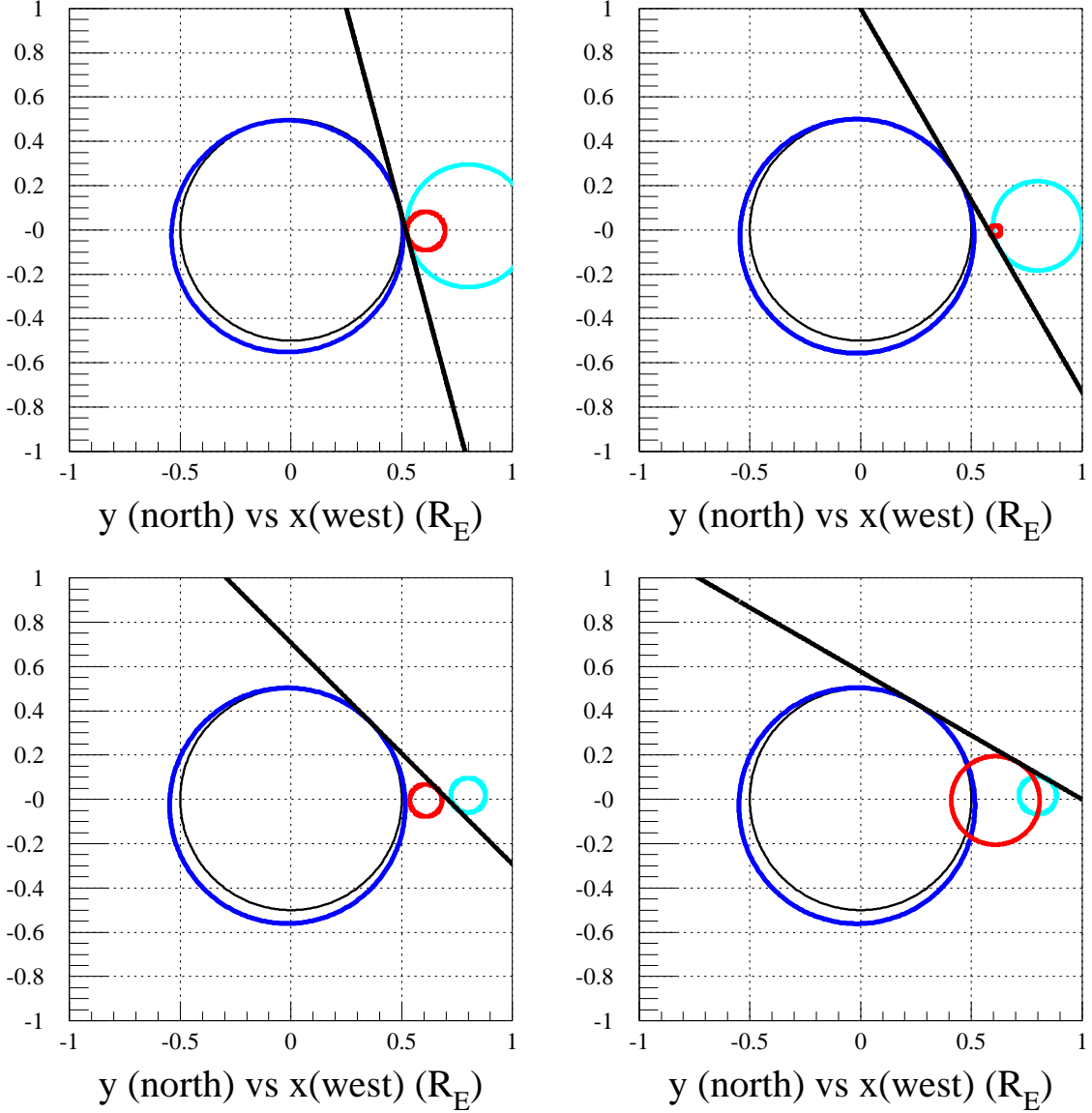


Fig. 7.— Projected in the lens plane, in an heliocentric reference frame centered on the line of sight to the source, the configurations, for four different lens trajectories, for a parallax microlensing event for three observers at rest, Earth, *Spitzer* and K2, for a line of sight towards the Bulge (see Section 4 for full details). The thin black circle is centered on the origin, radius the impact parameter as would be seen from the Sun. The thick circles are centered on the observer positions, with radius the respective impact parameters, dark, light blue and red for Earth, *Spitzer* and K2. The straight line represents the lens trajectory, simultaneously tangent to all the circles. The reference frame is as in Figure 1.

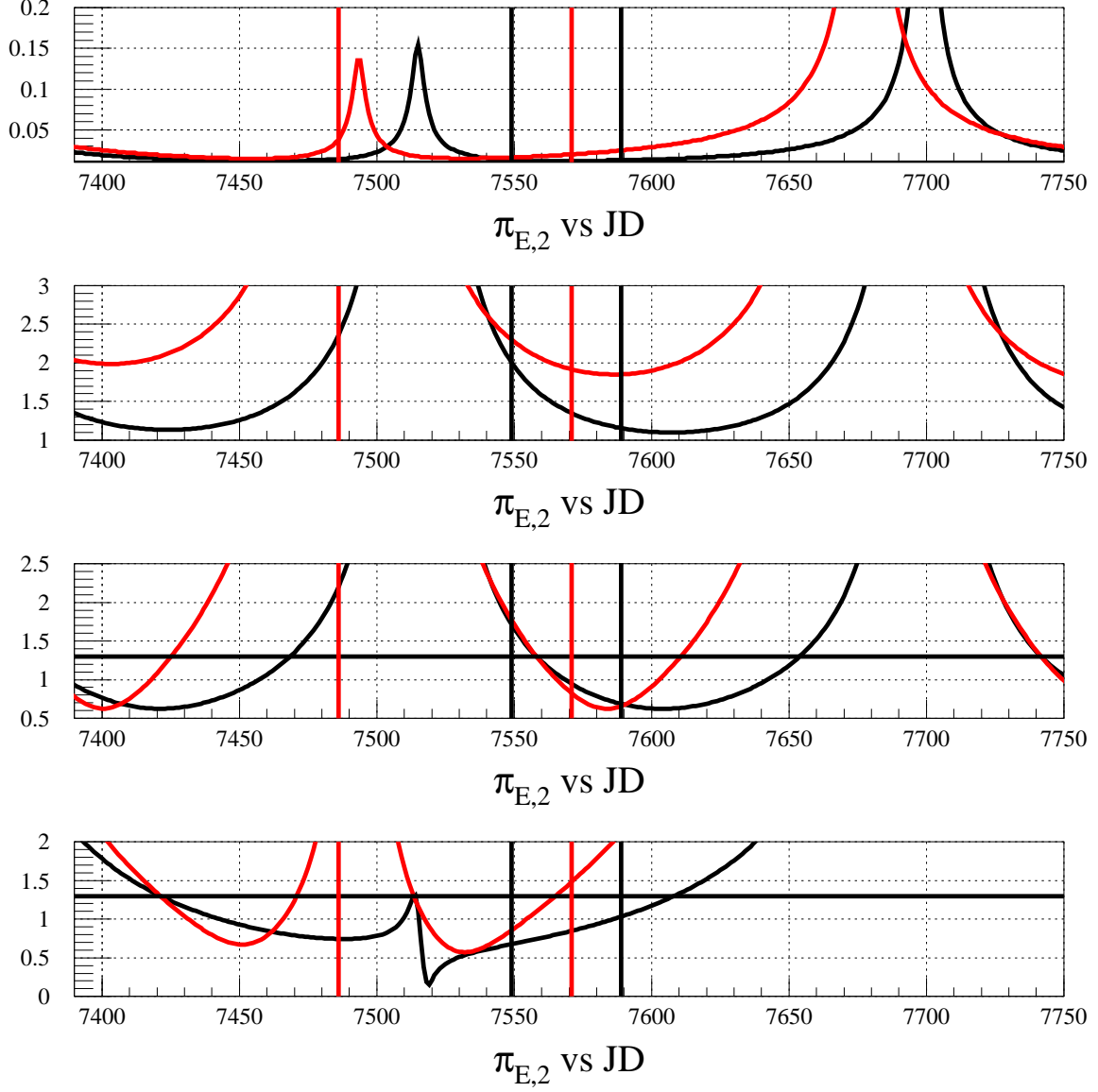


Fig. 8.— The degenerate value of the amplitude of the microlens parallax,  $\pi_{E,2}$ , for a given event configuration as a function of the time at maximum magnification fixed at the date of the day of the year 2016, as measured from *Spitzer* and K2, black and red lines, observers at rest. The horizontal lines indicate the true value of the amplitude of  $\pi_E$ . Two top (bottom) panels for  $\pi_E = 0.01$  (1.3), first and third (second and fourth) panels from top for  $u_0 = 0.01$  and 0.8, respectively. The vertical lines delimit the 2016 *Spitzer* and K2 campaigns. We refer to Section 4 for full details.